Remaining Useful Life for Heavy-Duty Railway Cast Steel Knuckles Based on Crack Growth Behavior with Hypothetical Distributions

Chao Wang[1] , Tao Zhu[1*], Bing Yang[1], Shoune Xiao[1] and Guangwu Yang[1]

Abstract

The current research on the integrity of critical structures of rail vehicles mainly focuses on the design stage, which needs an effective method for assessing the service state. This paper proposes a framework for predicting the remaining useful life (RUL) of in-service structures with and without visible cracks. The hypothetical distribution and delay time models were used to apply the equivalent crack growth life data of heavy-duty railway cast steel knuckles, which revealed the evolution characteristics of the crack length and life scores of the knuckle under different fracture failure modes. The results indicate that the method effectively predicts the RUL of service knuckles in different failure modes based on the cumulative failure probability curves for different locations and surface crack lengths. This study proposes an RUL prediction framework that supports the dynamic overhaul and state maintenance of knuckle fatigue cracks.

Keywords Heavy-duty railway, Cast steel knuckle, Remaining useful life, Fatigue crack growth, Hypothetical distribution

1 Introduction

With the gradual development of railway vehicles for heavy-duty and rapid transport, the service conditions of crucial vehicle components are gradually deteriorating, and higher requirements for their service safety and reliability [1–3]. The existing maintenance system for railway freight vehicles focuses on daily inspections, regular maintenance, and planned preventive maintenance [4]. Although this system can ensure the safe operation of vehicles, it will result in excessive maintenance and unnecessary maintenance costs. The overhaul mode based on condition monitoring data is widely used in energy, aerospace, rail transit, and other industrial fields owing to its forward-looking nature, high overhaul efficiency, safety, and reliability [5, 6]. Condition monitoring of the critical components of heavy-duty railway vehicles is a passive operation conducted under harsh environments and complex conditions. Owing to the incomplete monitoring methods, the lack of process monitoring for internal damage to system structures has increased the difficulty of realizing fault diagnosis and identification based on the service status.

The heavy-duty cast steel coupler is crucial for connecting and transmitting longitudinal forces between the locomotive head and the vehicle and between two vehicles. Specific results have been reported for the dynamic characteristics of heavy-duty coupler systems and the analysis of the vehicle dynamics performance. The coupler is affected by the bending moment caused by the height difference of the coupler, the lateral force

*Correspondence:
Tao Zhu
zhutao034@swjtu.edu.cn
[1] State Key Laboratory of Rail Transit Vehicle System, Southwest Jiao tong University, Chengdu 610031, China

caused by the lateral swing and shaking of the head, and the longitudinal impact caused by the gap of the coupler [7, 8]. At the same time, the fatigue performance of the coupler structure is also an essential factor affecting life expectancy. The casting process produces random individual defects, such as surface pores and inclusions. The randomness and stress redistribution of the contact relationship caused by the wear of the contact part of the coupler, incomplete non-destructive surface crack testing, and uncertainty regarding the crack size result in a very high dispersion of the service life of the coupler [9, 10]. Establishing a prediction model for the remaining useful life (RUL) takes much work. To perform a life assessment based on the service state of the structure, a test study based on the equivalent load can effectively reflect the condition damage process of the structure and predict the RUL of the equivalent service state of the vital structure [11, 12]. In terms of predicting the RUL of the railway vehicle structure, simulation methods are frequently used to investigate the crack growth behavior and RUL under specific damage and crack conditions [13–15]. In addition, it is difficult to establish a uniform crack growth model due to the service environment and the randomness of the crack state.

The critical components of heavy-duty railway vehicles are robustly designed and regularly maintained. When detected during inspections, cracks are repaired or replaced, and the residual value of damaged structures still needs to be effectively utilized. With the gradual improvement in testing and monitoring methods, more research has been carried out based on the reliability data analysis method for the life prediction of crucial components [16]. In the study on life predictions based on coupler failure data, Yin et al. [17] obtained the curve for the relationship between the reliability of the coupler body and the service mileage through a reliability analysis of a small sample of failure data obtained through fatigue bench tests of the coupler. The manuscript only reports the life distribution of one fracture failure mode and does not describe its multi-site cracking. Ren et al. [18] evaluated the RUL of a heavy-duty coupler for a railway freight car with initial defects based on a fracture mechanics approach. The life assessment was limited to 10000 tons of load as a simulation, and the results were not verified experimentally. The RUL prediction of crack growth life in a complex mechanical system needs to be more thorough. In the reliability life assessment of section crack growth behavior, analytical methods and applications based on equivalent service states have not been developed to achieve life prediction under multiple failure modes [19, 20], and an RUL prediction framework for the service crack growth process has not been established.

At the same time, the overall flow chart of the methodology used in this paper is necessary, as shown in Figure 1. A hypothetical distributed RUL prediction framework was proposed for visible and invisible cracks in service structures. The novelty is that the RUL distribution of different failure modes of complex structures is predicted based on the cumulative failure probability curve differently, and it is applied to the evolution of nondestructive testing cracks and life prediction under the equivalent service load of the heavy-duty railway knuckles. With new life data, the service mileage, crack location, crack size, and reliability are used as inputs to predict the RUL of the vital structural components based on the service status.

2 Experimental Procedures

2.1 Equivalent Service Fatigue Life Crack Growth Test

Heavy-duty railway wagons have a variety of structural forms, and typical coupler structures include 16-type rotary cast steel couplers and 17-type cast steel couplers, both of which are made of E-cast steel [9, 17]. The couplers have the advantages of a small connecting gap, high structural strength, good interlocking performance, and high vertical anti-falling performance. They are currently mainly used on 70-ton and 80-ton heavy-duty railway vehicles. The 16H knuckle in the middle cavity connects the two couplers, and the traction pins at both ends of the knuckle are connected to the vehicle under the frame to realize the transmission of traction between the vehicles. The failure rate of coupler cracks continues to increase under the action of a large traction impact load. For the knuckle, the crack rate is as high as 60%−70%, generally occurring on the upper and lower traction platforms and the S traction surface of the knuckle. The composition of the coupler system, crack rates, and location of the knuckle during actual service are shown in Figure 2.

The service load studied in this work is 20000 tons of heavy-duty railway. Among them, the service load spectrum is derived from the coupler force obtained from the actual formation test, including operational factors such as traction braking during the vehicle formation operation. The bench test of the equivalent service life is carried out based on actual service conditions, considering the marshaling and coupler force during the actual service of the coupler. At the same time, the comprehensiveness of the test sample and the consistency of the distribution pattern of fault locations are ensured. The test samples and fracture failure patterns were statistically analyzed, as shown in Figure 3.

Two fracture failures were observed during fatigue bench testing of the knuckle: a fracture of the lower traction platform and a fracture of the S traction surface. The coexistence of the two parts of the cracks during the test
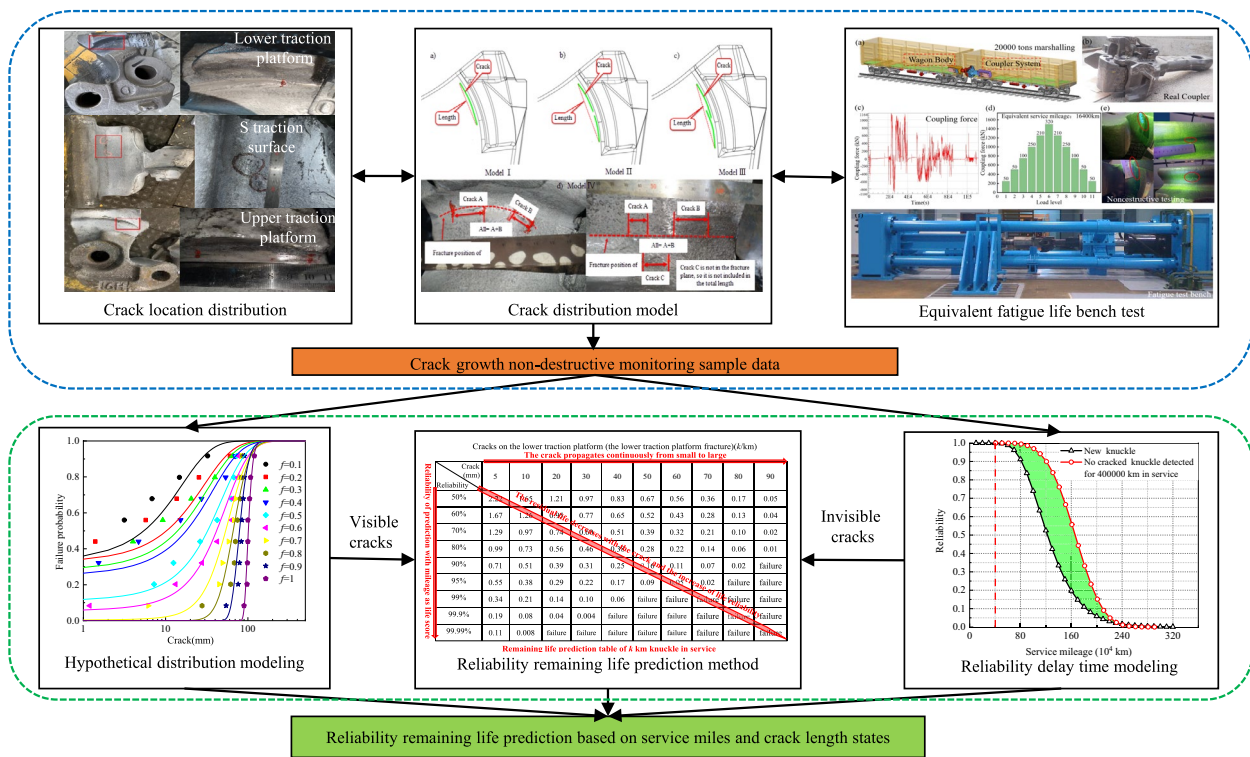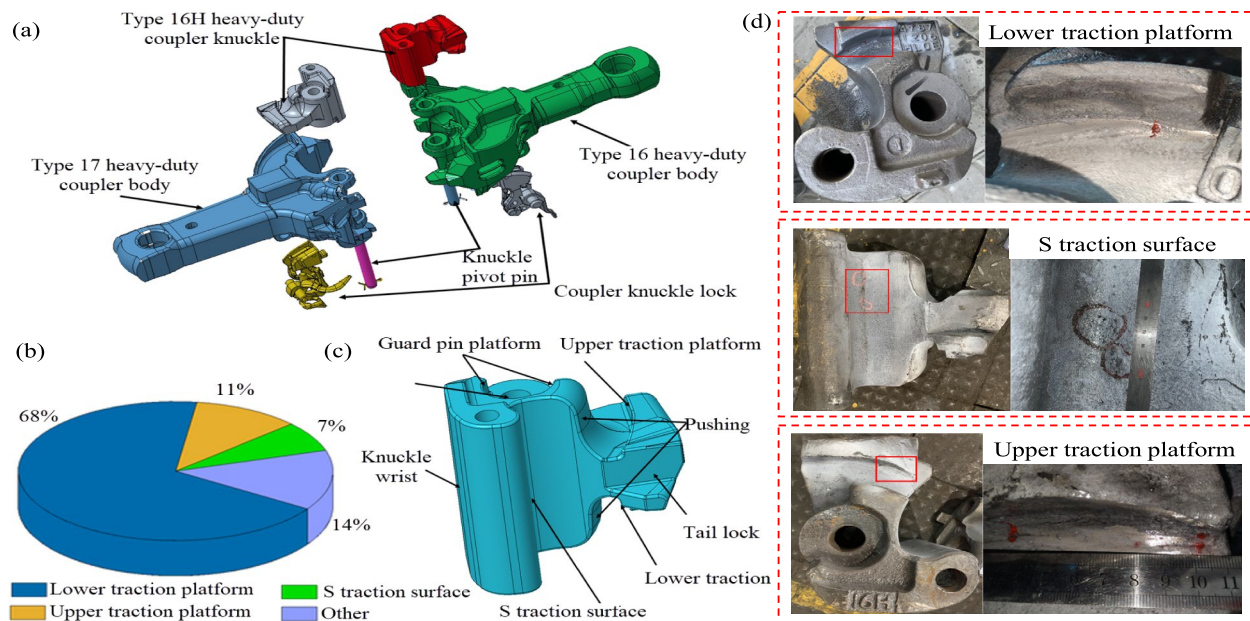
Figure 1 The overall flow chart of the methodology

Figure 2 Heavy-duty coupler composition and crack location distribution: (**a**) Composition of heavy-duty couplers, (**b**) Proportion of knuckle crack distribution locations, (**c**) Name of knuckle parts, (**d**) Location of solid cast knuckle cracks
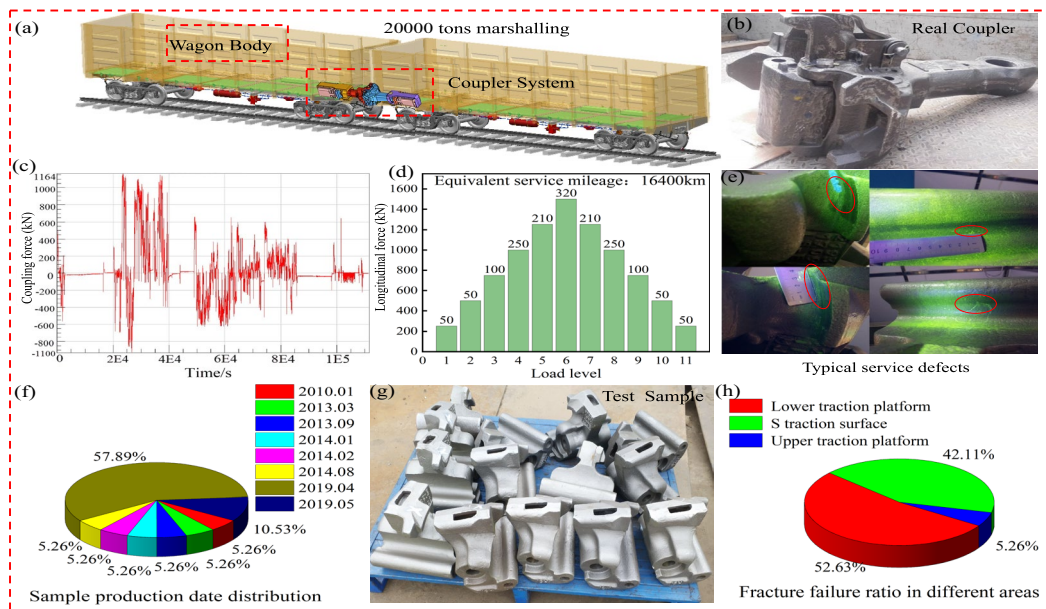
Figure 3 Equivalent service load and test knuckle samples: (**a**) Heavy vehicle marshalling model (**b**) Heavy duty casting coupler structure, (**c**) Coupler force load spectrum, (**d**) Equivalent service fatigue bench test load spectra, (**e**) Non-destructive testing for cracks in service knuckles, (**f**) Knuckle test sample date distribution, (**g**) Knuckle test sample, (**h**) Fracture failure ratio of knuckle at different areas
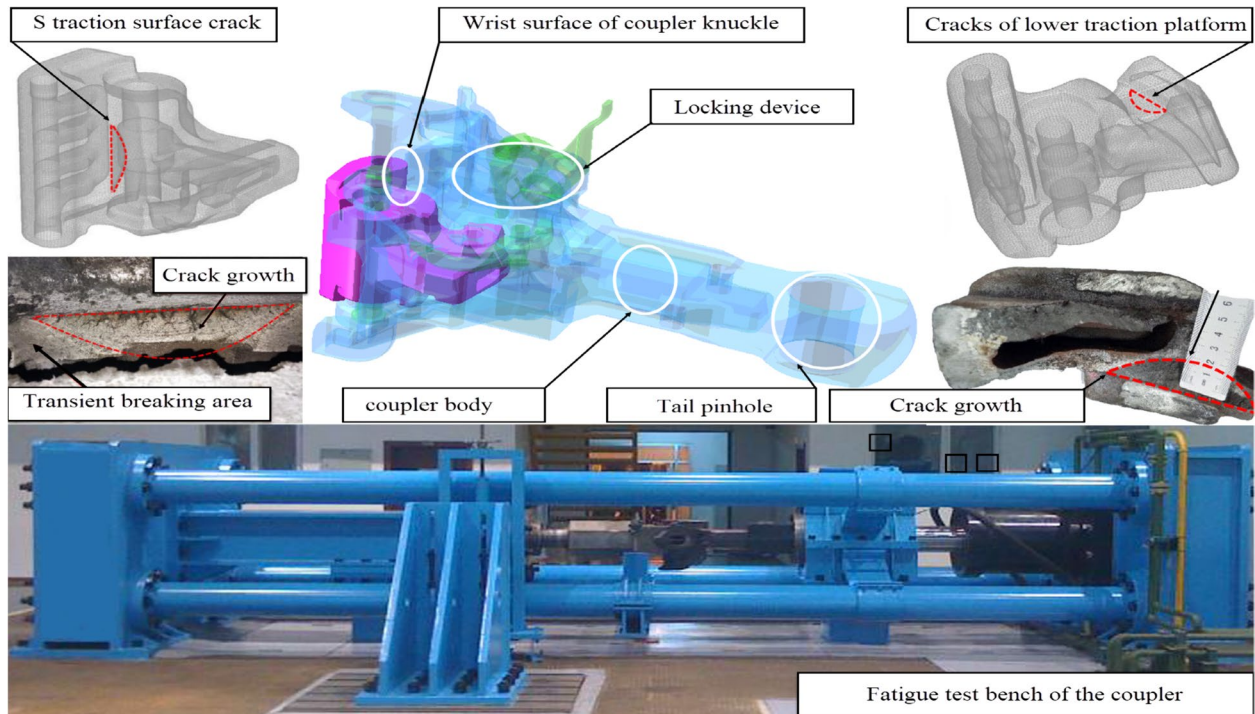

Figure 4 Failure modes of the knuckle and the fatigue test bench

indicates two fracture failure results. Figure 4 shows the fatigue crack growth behavior and fatigue failure region of the knuckle.

The results of the fatigue tests show that the failure of the knuckle is mainly due to instantaneous fracture of the surface cracks at the root of the lower traction platform
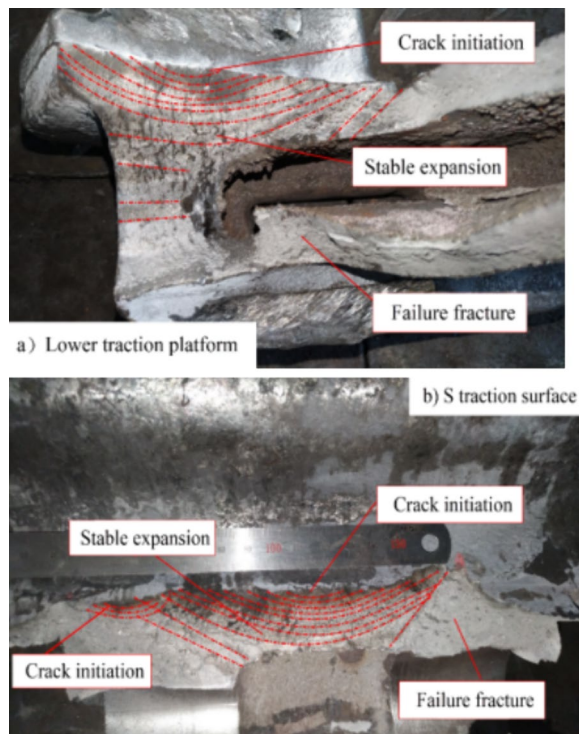
Figure 5 Typical fracture failure modes of fatigue crack growth in the knuckle: (**a**) Fracture of the lower traction platform under the knuckle (**b**) S traction surface under the knuckle

Figure 6 Equivalent crack patterns in different regions of the knuckle: (**a**) Equivalent crack Model I, (**b**) Equivalent crack Model II, (**c**) Equivalent crack Model III, (**d**) Equivalent crack Model IV

or the S traction surface under fatigue cyclic loading. These cracks expand to the size of the fracture crack, which can be observed from a macroscopic perspective. The morphology of the knuckle fracture is a typical fatigue failure fracture, with a crack source, a "beach strip" fatigue crack growth zone, and an instantaneous fracture zone. The typical crack growth fracture failure locations and shapes are shown in Figure 5.

2.2 Definition of the Crack Size Model

Based on the actual service status, it is necessary to conduct a fracture failure study of the fatigue crack growth behavior of the structure through equivalent tests, which can be used to predict the RUL of the structure. Considering the complexity of the knuckle structure of the heavy-duty railway and the defects of the casting process, the crack growth process of the knuckle structure is not a main crack. Under the action of fatigue load, the knuckle structure is accompanied by the initiation of several small cracks in the early stage, which finally merge into a main crack and propagate to failure. In order to facilitate the recording of the crack length and the statistical analysis for crack growth on the weak part of the knuckle (root arc of the upper traction platform arc, root arc of the lower traction platform, S straight line in the middle of
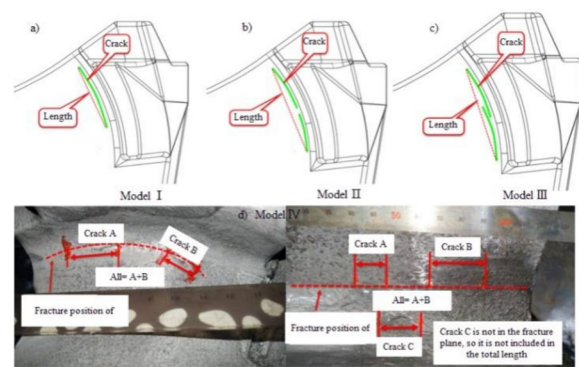
the traction surface), the following four crack size models are defined.

Based on the multiple crack coplanarity and merging criterion in the safety assessment criteria for defect-containing structures, the coplanarity criterion is applied for two neighboring cracks to merge them into one main crack. Multiple cracks in different knuckle regions were defined as four equivalent crack patterns [21, 22]. Model I: In the case of a single crack, the straight-line distance between the start and end of the crack is defined as the crack length. Model II: The distance between the two cracks is less than 5 mm, and the two cracks are merged into one crack. Model III: Two cracks are parallel (closer distance) and partially overlapped, the overlapped part and parallel distance are ignored. Model IV: If there are n collinear cracks and the distance between the cracks is greater than 5 mm, the crack sizes are recorded separately, and the total length of the crack is defined as the sum of n cracks. The equivalent crack size models at different parts are shown in Figure 6.

2.3 Equivalent Test Verification

The overhaul period of a knuckle is approximately 400000 km in service. First, the service load of the coupler was obtained according to the actual service state of the line, and then the bench test load spectrum was obtained. Based on the equivalent service load, the fatigue bench test of the new knuckle was carried out, and the fatigue cracks of the structure at different positions under the action of the fatigue load were monitored. The corresponding relationship between different crack lengths and the number of fatigue load cycles was recorded from crack initiation to final fracture failure. Finally, the life data of the knuckle of a limited sample were obtained. The mileage and bench test load spectra are equivalently converted to obtain the bench test
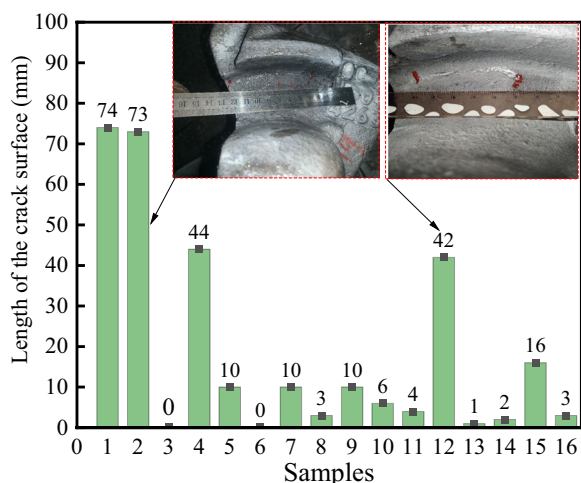
Figure 7 Length of crack on the surface of the lower traction platform under the test knuckle

Table 1 Fitting parameters of crack length with normal distribution

	Mean (mm)	Standard deviation (mm)	Coefficient variation	Correlation coefficient
Actual service	18	21	1.1795	0.8811
Equivalent test	19	25	1.1303	0.8406

knuckle after approximately 40000 fatigue cycles. Therefore, according to the crack sizes of different parts corresponding to the equivalent service mileage of the bench test, the crack information for 16 test knuckles in this cycle is obtained, as summarized in Figure 7.

According to the bench test load history of the knuckle in the equivalent service period corresponding to one repair period in Figure 7, the crack size of the lower traction platform is fitted to a normal distribution, and the data for the knuckle cracks in the actual service are obtained during a repair period. The fitting results are compared, and the mean, standard deviation, coefficient of variation, and correlation coefficient of the two fitted datasets are listed in Table 1.

The correlation coefficients of the two fitting models are more significant than 0.8, indicating that the normal distribution can satisfactorily fit the crack data of the test equivalent knuckle in service for a period of service. The coefficient of variation is relatively large, indicating that the data dispersion is relatively large. Based on the mean values, the test knuckle was used for a period equivalent to the maintenance period, and the length of the cracks on the lower traction platform was approximately 19 mm. In the survey data, the average crack length on the lower traction platform was approximately

18 mm, and the average value in the actual service was slightly lower. The main reason is that the load spectrum used in the test is equivalent to a relatively harsh knuckle position. In contrast, the knuckle position in the field investigation was random. In summary, the fatigue test of the coupler is conservative compared with the actual service condition of the line and can adequately meet the actual safety requirements of the project. Moreover, the test results can reflect the cracking condition of the service state of the knuckle to a certain extent. Therefore, the subsequent analysis is based on the crack growth test data of the knuckle to develop a prediction method for the RUL.

3 Remaining Useful Life Prediction with Visible Cracks

3.1 Hypothetical Distribution Evaluation Method

The hypothetical distribution is a statistical hypothesis of random variables, which can effectively describe the random distribution of system failure data and predict component life by fitting failure data under different failure modes [23]. Based on the assumed distribution and improved model, many research fields have applied the parameter estimation method for failure samples under complex conditions [24, 25]. In mechanical system structure, the reliability index refers to the probability that the structure will complete a predetermined function under specified conditions and time. Commonly used reliability indicators include reliability, failure rate, and average working time. Assuming that the probability density function is $f(t)$, the reliability $R(t)$ is defined as the probability that the service life is greater than a certain specified value t, as shown in Eq. (1):

$$R(t) = \int_t^\infty f(t)\mathrm{d}t, t \geq 0. \tag{1}$$

The cumulative failure probability is defined as shown in Eq. (2):

$$F(t) = 1 - R(t). \tag{2}$$

The key to calculating the structural reliability is obtaining the structural failure probability density function $f(t)$, for large-sample problems (capacity of more than 50 or 70), as the probability density function is generally determined directly based on the data. For small-sample problems, the overall fitting effect, fatigue failure mechanism, and algorithm safety can be comprehensively considered. Commonly used statistical distribution types include the three-parameter Weibull distribution (3PWD), two-parameter Weibull distribution (2PWD), normal distribution (ND), lognormal distribution (LND),

minimum value distribution (EMVD1), maximum value distribution (EMVD2), and exponential distribution (ED) [26–28]. A suitable hypothetical distribution is selected as follows:

a) The data were sorted from smallest to largest and the empirical failure probability was calculated based on the median $P_{em}(x_i)$:

$$P_{em}(x_i) = \frac{i - 0.3}{n + 0.4}, i = 1, 2, 3...n. \tag{3}$$

b) Based on linear regression, the common statistical distributions are used to fit the data $(x_i, P_{em}(x_i))$, and the statistical distribution parameters and fitting correlation coefficients R_{XY} is obtained.

c) For high reliability, the safety of the tail prediction can be evaluated by d_{F1} and d_{F2}.

For the left tail, the equations are as follows:

$$d_{F1} = P_{em}(x_1) - P_{th}(x_1), \tag{4}$$

$$d_{F2} = P_{em}(x_2) - P_{th}(x_2). \tag{5}$$

For the right tail, the equations are as follows:

$$d_{F1} = P_{em}(x_n) - P_{th}(x_n), \tag{6}$$

$$d_{F2} = P_{em}(x_{n-1}) - P_{th}(x_{n-1}). \tag{7}$$

Considering the fitting correlation coefficient, fatigue failure mechanism, and safety of the tail prediction comprehensively [29]. The above hypothetical distributions are used as the hypothetical distribution of crack length under a specific life score. The goodness of fit test is carried out on the crack size based on the hypothesized distribution. The linear correlation coefficients under each distribution function are compared to judge whether the hypothesized distribution is reasonable. The cumulative failure probability curve of the structure is obtained to realize the RUL prediction based on the overall characteristics.

3.2 Distribution Fitting RUL Results
During the knuckle equivalent service load fatigue bench tests, two crack growth behaviors occur under the same fracture failure mode: crack growth on the lower traction platform and the S traction surface. The RUL is defined as the period from the fatigue load cycle life of

Table 2 Evolution of the crack length on the lower traction platform with the life score

Life score	Mode I crack length (mm)								Mode II crack length (mm)							
	#1	#2	#3	#4	#5	#6	#7	#8	#9	#10	#11	#12	#13	#14	#15	#16
0.1	6.8	32.4	0.0	14.7	0.0	0.0	3.1	0.0	1.6	0.8	1.0	3.4	0.5	0.9	0.9	1.2
0.2	13.7	60.7	0.0	25.4	0.0	0.0	5.7	1.4	16.3	2.5	3.0	36.2	1.0	1.7	2.7	7.0
0.3	20.5	65.6	0.0	39.8	0.0	0.0	9.2	4.0	22.8	8.8	5.0	47.1	1.5	3.7	30.4	41.3
0.4	27.3	69.9	0.0	53.8	1.5	0.0	15.2	4.7	27.3	23.9	39.9	51.4	2.0	11.1	63.8	52.6
0.5	67.6	73.2	42.4	62.9	12.5	0.0	26.2	7.2	33.3	35.4	47.1	60.1	2.9	20.3	73.1	61.3
0.6	77.4	75.8	63.6	65.5	27.7	1.2	42.4	13.2	38.7	36.8	48.1	61.2	3.9	22.7	74.0	90.2
0.7	84.1	77.6	67.8	71.5	58.3	6.2	49.1	44.8	40.5	40.4	50.7	64.1	7.0	36.4	74.9	92.1
0.8	86.7	83.6	70.7	74.7	80.8	27.8	61.9	68.6	59.5	50.0	66.5	66.2	10.4	37.8	79.3	93.3
0.9	91.2	90.6	76.4	79.4	83.3	54.5	85.0	88.2	73.9	52.6	71.5	69.0	11.5	47.3	80.8	97.5
1	108.0	105.0	98.0	90.0	100.0	99.0	100.0	120.0	76.0	80.0	77.0	81.0	12.0	53.0	82.0	106.9
Life score	Mode III crack length (mm)								Mode IV crack length (mm)							
	#1	#2	#3	#4	#5	#6	#7	#8	#14	#15	#16	#17	#18	#19	#20	#21
0.1	3.2	0.3	1.0	0.6	7.8	0.4	0.4	0.3	6.8	0.9	1.4	41.2	0.0	0.0	2.5	7.7
0.2	6.3	0.5	1.5	1.0	15.0	0.6	0.7	0.6	8.7	2.7	5.5	44.0	0.0	0.0	13.0	15.4
0.3	9.5	0.8	2.0	1.8	15.6	0.8	0.9	0.8	9.6	6.8	18.0	51.8	25.3	14.3	19.0	21.9
0.4	12.7	1.1	3.0	2.5	16.1	1.0	1.1	0.9	10.8	12.5	86.1	56.6	32.5	41.0	35.0	27.1
0.5	15.0	1.3	16.2	3.6	16.6	1.3	1.5	1.2	12.8	30.1	97.6	58.8	48.9	58.9	49.1	32.9
0.6	15.6	1.6	21.7	5.1	17.1	1.6	1.9	1.5	15.2	31.0	120.5	76.1	69.2	81.5	61.0	43.3
0.7	16.2	1.9	26.6	5.8	17.6	1.9	2.3	1.9	16.9	31.9	125.5	100.0	83.8	100.1	72.3	51.4
0.8	16.6	2.4	52.5	6.6	18.1	2.3	2.7	2.4	85.2	83.1	130.2	108.7	100.1	116.5	94.2	63.6
0.9	17.1	3.0	64.0	7.3	18.7	2.7	3.1	3.1	120.2	129.1	133.0	117.0	117.2	126.6	119.6	94.9
1	18.0	4.0	120.0	9.0	20.0	4.0	4.0	4.0	145.0	150.0	140.0	141.0	130.0	140.0	140.0	110.0
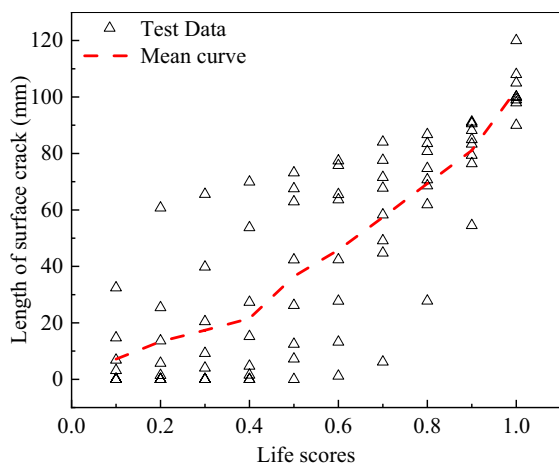
(a) Variation in the mean value
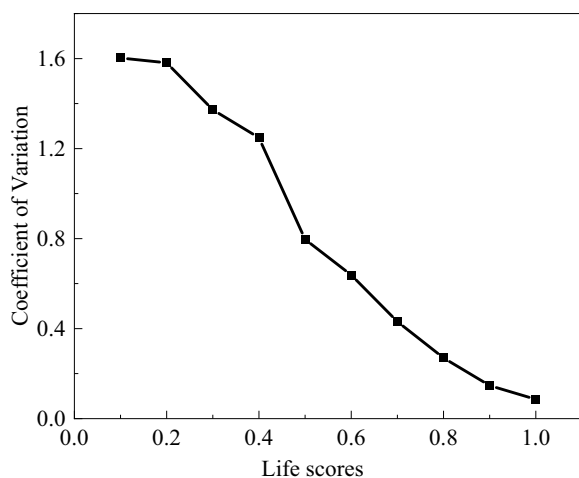
(b) Coefficient of variation trend

Figure 8 Relationship between crack length and variation

the structure with a certain crack size to the final failure. Based on bench test data, the life score is defined as the ratio of fatigue loading cycles at the structure's current crack length to the cycles at fracture failure. The life score is distinguished for crack growth on these two parts under the fracture failure modes. The following four crack growth behavior modes are defined: Mode I: Lower traction platform cracks under a lower traction platform fracture; Mode II: Lower traction platform cracks under an S traction surface fracture; Mode III: S traction surface cracks under a lower traction platform fracture; Mode IV: S traction surface cracks under an S traction surface fracture. In order to facilitate the analysis of the fracture behavior, the surface crack lengths with identical life scores under the four modes are calculated through linear interpolation, as summarized in Table 2.

Taking the Mode I life score data (samples #1−#8) as an example, the calculated curve in the average crack length and the variation coefficient are shown in Figure 8.

According to the crack growth behavior of the lower traction platform in Mode I, the mean value increases continuously with the increase in the life score. However, the coefficient of variation steadily declines, moving from a strong to a weak variation. This demonstrates that the crack length exhibits considerable dispersion at the initial crack growth stage. However, the dispersion steadily decreases as the crack length increases. Combining the structure and measurement error of the crack definition and length during the growth process indicates that in the initial stage of crack growth, multiple small cracks are generated at the stress concentration area at the root of the traction platform, and the randomness of the locations and sizes of these tiny cracks leads to high dispersion. Under cyclic loading, the position of the fracture becomes relatively fixed as the minor cracks progressively merge to form the significant fatigue crack, and the

Table 3 Fitting correlation coefficients for the crack length under each hypothetical distribution

Life score	Fitting correlation coefficient					
	3PWD	2PWD	ND	LND	EMVD1	EMVD2
0.1	–	–	0.8407	–	0.7543	− 0.9126
0.2	–	–	0.8410	–	0.7549	− 0.9123
0.3	–	–	0.8906	–	0.8133	− 0.9480
0.4	–	–	0.9133	–	0.8454	− 0.9572
0.5	–	–	0.9666	–	0.9496	− 0.9534
0.6	0.9242	0.9242	0.9652	0.8578	0.9757	− 0.9267
0.7	0.8665	0.8665	0.9415	0.7943	0.9771	− 0.8879
0.8	0.8897	0.8897	0.8965	0.8227	0.9464	− 0.8317
0.9	0.9175	0.9175	0.8894	0.8555	0.9430	− 0.8199
1	0.9569	0.9237	0.9456	0.9544	0.9079	− 0.9693

Table 4 The failure probability predicted differences of six hypothetical distributions

Life score	3PWD		2PWD		ND		LND		EMVD1		EMVD2	
	d_{F1}	d_{F2}	d_{F1}	d_{F2}	d_{F1}	d_{F2}	d_{F1}	d_{F2}	d_{F1}	d_{F2}	d_{F1}	d_{F2}
0.1	–	–	–	–	−0.036	0.106	–	–	−0.059	0.154	−0.019	0.064
0.2	–	–	–	–	−0.039	0.131	–	–	−0.061	0.181	−0.021	0.085
0.3	–	–	–	–	−0.031	0.023	–	–	−0.056	0.050	−0.012	0.000
0.4	–	–	–	–	−0.014	−0.041	–	–	−0.040	−0.038	0.004	−0.045
0.5	–	–	–	–	0.052	−0.027	–	–	0.026	−0.039	0.065	−0.024
0.6	0.214	0.100	0.214	0.100	0.091	−0.016	0.211	0.096	0.068	−0.034	0.099	−0.011
0.7	0.239	0.152	0.239	0.152	0.097	0.042	0.231	0.136	0.068	0.037	0.106	0.035
0.8	0.210	0.127	0.210	0.127	0.143	0.067	0.209	0.116	0.126	0.067	0.144	0.057
0.9	0.191	0.087	0.191	0.087	0.165	0.059	0.193	0.085	0.155	0.054	0.161	0.051
1	−0.036	0.081	−0.067	0.110	−0.038	0.095	−0.033	0.083	−0.070	0.127	−0.013	0.063

Table 5 Parameters of the cumulative distribution functions for four failure modes

Life score	EMVD2 (Mode I)		EMVD1 (Mode II)		3PWD (Mode III)			EMVD1 (Mode IV)	
	Location parameter	Scale parameter	Location parameter	Scale parameter	Shape parameter	Location parameter	Scale parameter	Location parameter	Scale parameter
0.1	1.2392	11.4796	1.8230	1.0641	0.4412	0.2666	0.7943	4.5130	3.4335
0.2	2.4695	21.2021	16.5764	15.1394	0.3788	0.5377	1.1422	9.5718	6.0907
0.3	5.5442	23.0431	29.3483	18.0484	0.2643	0.8043	0.9225	19.5454	6.1878
0.4	8.3311	25.7253	44.3566	20.1500	0.3398	0.9379	1.7436	50.4550	24.7913
0.5	22.1455	27.9071	52.7495	21.5499	0.3360	1.1827	3.2461	61.3984	24.8520
0.6	30.9910	28.9049	60.2887	25.9462	0.3189	1.5203	3.5699	78.2654	31.1785
0.7	44.3077	25.5013	63.4891	24.7426	0.3146	1.8573	3.8604	90.4582	34.4697
0.8	58.7523	20.5928	70.0053	23.5999	0.3163	2.2945	4.6588	107.7129	19.4828
0.9	74.2319	13.3026	75.4920	24.3021	0.3745	2.6432	6.2956	126.4937	6.4011
1	98.2206	8.3245	83.8299	26.4167	0.3481	3.8468	7.5177	143.9186	6.0256

measurement error is minimized, resulting in less dispersion in the data in the later stage.

A comparative analysis using the following procedures should determine an appropriate hypothetical distribution: checking the total fit effects of possible assumed distributions on the crack length under a specific life score data. The approach allows consistency with the fatigue physics and checks tail fit effects. The six parameter distributions listed above are considered hypothetical distributions of the crack length under a specific life score and the linear correlation coefficients of each distribution function. Finally, the R_{XY} values for each set of data are compared. The fitted linear correlation coefficients for the hypothetical distributions are listed in Table 3.

As shown in Table 4, the $|R_{XY}|$ value closer to 1 indicates a higher degree of fit. No data are available for life scores below, it cannot be assumed that their distributions are 3PWD, 2PWD, or LND. From the perspective of an $|R_{XY}|$ close to 1, EMVD2 provides the best fit for data with life scores of 0.1, 0.2, 0.3, 0.4, and 1. The ND function fitted best for data with a life value of 0.5, while EMVD1 fitted best for data with life values of 0.6, 0.7, 0.8, and 0.9. The data were further analyzed in terms of the safety of the tail prediction in order to obtain more reliable results. The deviations between the empirical value and the predicted value of the failure probability at the right tail of the six hypothetical distributions (d_{F1} and d_{F2}) are summarized in Table 4.

The results in Table 4 indicate that $d_{F1} < d_{F2}$ means that as the reliability increases, there is a tendency to be more conservative. For $d_{F1} < 0$, $x > x_n$ can provide a conservative estimate. For data that satisfy $d_{F1} < d_{F2}$, 3PWD has one group, 2PWD has one group, ND has four groups, LND has one group, EMVD1 has five groups, and EMVD2 has four groups. For data that satisfy $d_{F1} < 0$, 3PWD has one group, 2PWD has one group, ND has five

groups, LND has one group, EMVD1 has five groups, and EMVD2 has four groups [29].

Considering the degree of fit and the safety of the tail prediction, EMVD2 can be used as a good hypothetical distribution for the Mode I failure crack data. Based on the above analysis method, the parameters of the cumulative distribution functions of the four crack growth behaviors and fracture failure modes under different life scores can be obtained, as summarized in Table 5. The corresponding cumulative distribution curves are presented in Figure 9.

Considering the degree of fit and the safety of the tail prediction, different distributions can be used as good statistical distributions under different failure modes. Based on the given crack surface length and cumulative failure probability of the different failure modes in Figure 9, the RUL of the knuckle can be predicted. Taking failure Mode I as an example, the specific method is as follows: assuming that a knuckle has been in service for k kilometers, the root crack length of the lower traction platform is determined through flaw detection to

be 10 mm (corresponding to the transverse coordinates in Figure 9a). Then, for a cumulative failure probability of 0.1 (corresponding to the ordinate in Figure 9a), an evaluation point can be identified in Figure 9a, and this point falls in the middle of the curve with a life score of 0.6. This indicates that the service life is approximately 60% of the entire life, which is expected to be 1.67 k km, and the knuckle can thus still be used for 0.67 k km (k is a dimensionless unit). This conclusion has 90% reliability. The method for using the RUL cumulative failure probability curves under the other failure modes is the same. When high reliability is required (above 99.9%), a knuckle that has been in service for a repair period is tested for flaws. Once a crack (greater than 5 mm) is detected, the knuckle can be expected to survive the next repair period.

3.3 Validation of the Crack Growth Analysis
The crack growth analysis of a service-damaged knuckle selects two damaged knuckles under each of four failure modes. The crack growth curve of the new test knuckle
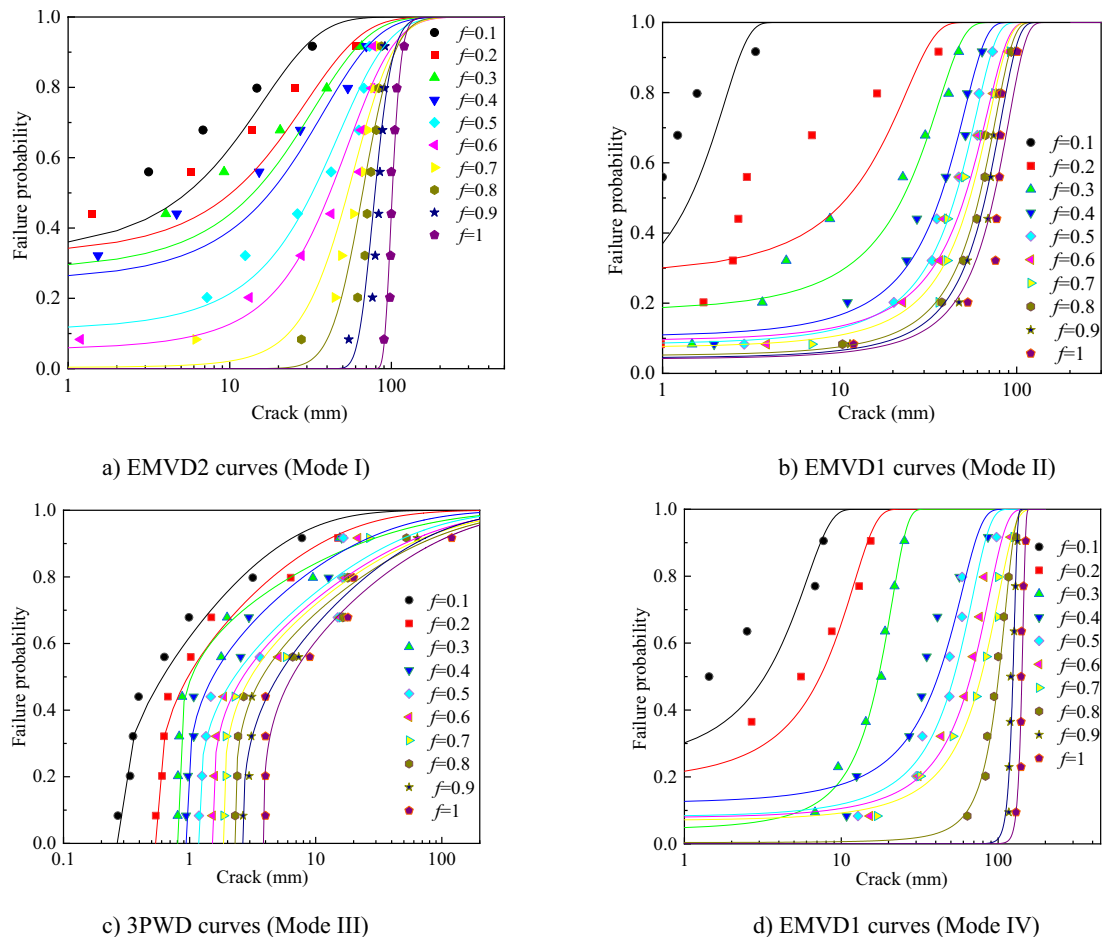

a) EMVD2 curves (Mode I)

b) EMVD1 curves (Mode II)

c) 3PWD curves (Mode III)

d) EMVD1 curves (Mode IV)

Figure 9 Cumulative distribution curves for the crack length with different life scores

is used to compare and verify the effectiveness of the fatigue crack bench test of the knuckle. The results of the comparison are shown in Figure 10.

For the knuckle with crack growth on the lower traction platform, the knuckle in the lower traction platform failure Mode I is shown in Figure 10(a). The crack growth curve of the damaged knuckle tends to be flat in the first half of the life scores. The crack length ratio to the life scores rises gradually from the life fraction of 0.6 onwards, and the overall trend is consistent with the new knuckle in the equivalent bench test. Similarly, the failure Mode II in Figure 10(b) is the same as that for Mode I. For the third failure mode, as shown in Figure 10(c), the crack growth occurs on the S surface of the knuckle and the lower traction platform at the same time, the appearance of cracks in the lower traction platform leads to a reduction in the overall stiffness of the knuckle, and the crack growth rate of the S surface is relatively flat. For the cracks in the S surface of the knuckle and finally breaks in this mode, the crack growth location is more centralized in a plane, and the crack growth curve of the damaged knuckle is similar to that of the new knuckle. As shown in Figure 10(d), it can be analyzed that the crack growth curve of the damaged knuckle agrees well with the equivalent bench test data of the new knuckle. Overall, the crack growth curve of the damaged knuckle is almost entirely within the dispersion zone of the new knuckle test data, and it is consistent with the trend of the crack growth curve of the new knuckle. Therefore, these results verify that the fatigue bench test of the knuckle can reflect the actual service status of the knuckle to a certain extent, and the results of the crack growth analysis of the knuckle based on the bench test can guide the implementation of the condition detection and maintenance.

4 Remaining Useful Life Prediction Invisible Cracks

Section 3 realizes the prediction of RUL for different failure modes based on the knuckle non-destructive monitoring of crack growth life data. When there is an invisible fatigue crack in the knuckle, it is considered that the structure is in the stage before crack initiation, and damage has been generated relative to the new knuckle. However, existing flaw detection means that internal damage cannot be quantified. The crack rate of a knuckle in service for 400000 km is approximately 60%–70%. Once cracks are found, they will be scrapped. In order to evaluate the condition of the knuckle, a guideline for extending the maintenance period is proposed. Determining the RUL of a knuckle that has been in service for 30%–40% invisible cracks are also essential. Based on the relationship between the crack growth life data and service mileage of different knuckle samples under the equivalent service load above, the reliability curve for a knuckle with
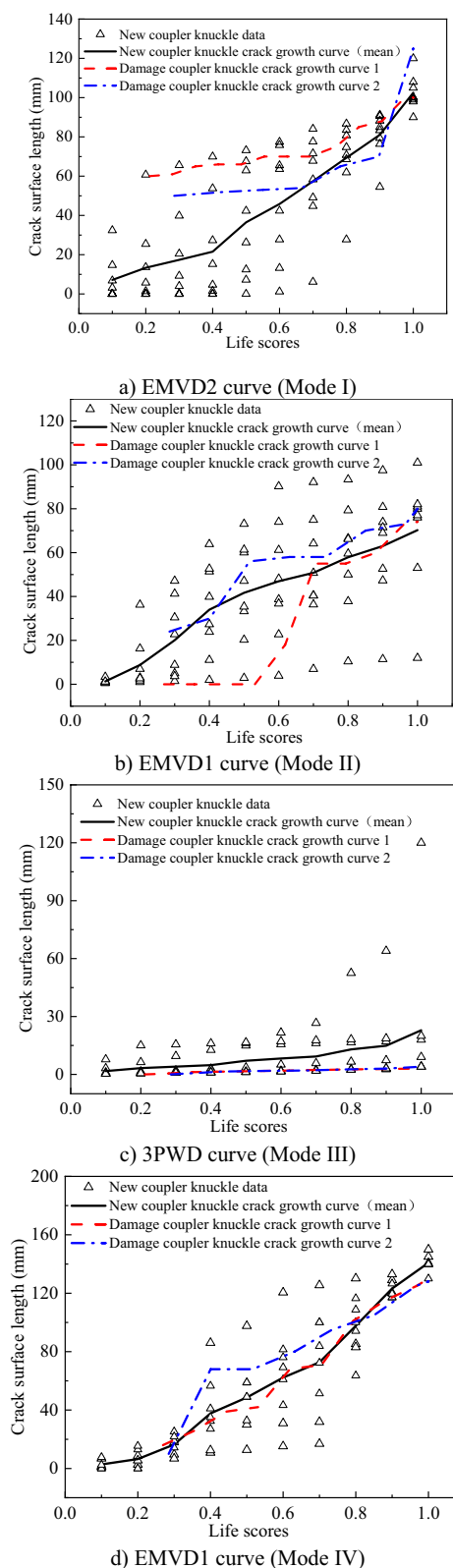

a) EMVD2 curve (Mode I)

b) EMVD1 curve (Mode II)

c) 3PWD curve (Mode III)

d) EMVD1 curve (Mode IV)

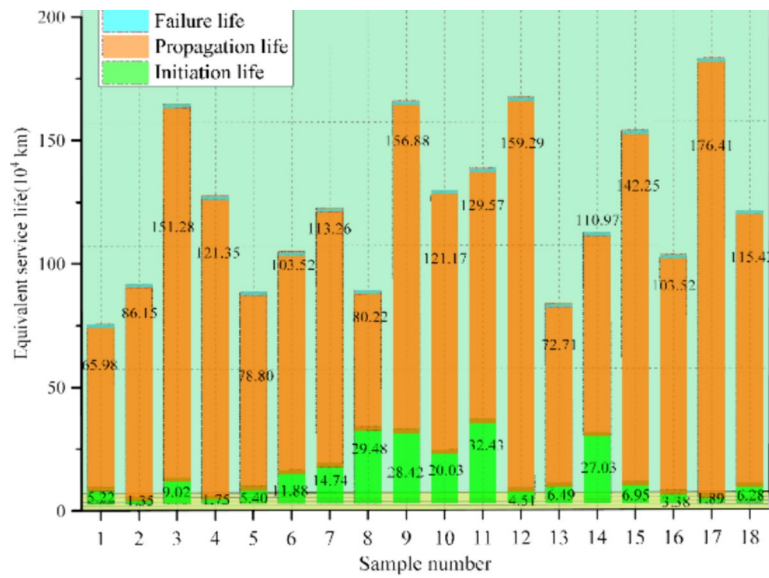**Figure 10** Comparative of life scores for damage knuckles

Figure 11 Equivalent life of knuckle crack growth results

400000 km of driving range and invisible cracks can be calculated as follows: considering the detection accuracy and dispersion of the surface defects of the structure, the whole process of structural service failure is divided into two stages. The surface crack length of 5 mm is defined as the crack initiation size, and the extension from 5 mm to critical failure is regarded as the growth life. The service mileage of the line corresponding to a surface crack length of 5 mm is obtained through linear interpolation, and the results are listed in Figure 11. The Grubbs test is used to ensure that there is no abnormal data in the life data for the knuckle crack initiation and growth life data [30, 31]. A two-parameter Weibull distribution is used to fit the life data. The fitting parameters of the life data are listed in Table 6.

The probability density function for the crack initiation life N_i is

$$f(N_i) = \frac{1.1244}{12.6995} \times \left(\frac{N_i}{12.6995} \right)^{1.1244-1} \exp\left[-\left(\frac{N_i}{12.6995} \right)^{1.1244} \right]. \tag{8}$$

The cumulative distribution function as:

$$F(N_i) = 1 - \exp\left[-\left(\frac{N_i}{12.6995} \right)^{1.1244} \right]. \tag{9}$$

The probability density function for the crack growth life of the knuckle can be calculated by:

$$g(N_p) = \frac{3.9694}{128.0482} \times \left(\frac{N_p}{128.0482} \right)^{3.9694-1} \exp\left[-\left(\frac{N_p}{128.0482} \right)^{3.9694} \right]. \tag{10}$$

Table 6 Two-parameter Weibull distribution fitting parameters for the knuckle crack life data

Life	Shape parameter	Scale parameter	Fitting correlation coefficient
Crack initiation life N_i	1.1244	12.6995	0.9718
Crack growth life N_p	3.9694	128.0482	0.9815

The cumulative distribution function is

$$G(N_p) = 1 - \exp\left[-\left(\frac{N_p}{128.0482} \right)^{3.9694} \right]. \tag{11}$$

Based on the cumulative distribution function of crack initiation and propagation, the RUL prediction model based on delay time is constructed [32, 33]. It is assumed that the failure mileage of the knuckle is $t \times 10^4$ km ($t > 40$). Event A is defined as follows: the knuckle does not detect cracks at 400000 km, and the crack initiation life of the knuckle is $\mu \in (40, t)$. Event B is defined as follows: the knuckle fails before time t, and the crack growth life of the knuckle is $\nu \in (0, t-\mu)$. $P(B|A)$ represents the reliability of the knuckle that has been in service for

Table 7 Remaining mileages with different reliability levels

Reliability	Total service mileage (10^4 km)	Remaining mileage (10^4 km)	Reliability	Total service mileage (10^4 km)	Remaining mileage (10^4 km)
50%	166	126	90%	121	81
60%	157	117	95%	108	68
70%	147	107	99%	86	46
80%	136	96	99.9%	67	27

400000 km invisible cracks are detected [34, 35]. Here, μ and ν are independent random variables.

$$P(B|A) = \frac{P(AB)}{P(A)} = \frac{\int_{40}^{t} f(\mu)G(t-\mu)\mathrm{d}\mu}{\int_{40}^{t} f(\mu)\mathrm{d}\mu}, \qquad (12)$$

$$G(t-\mu) = \int_{0}^{t-\mu} g(\nu)\mathrm{d}\nu. \qquad (13)$$

According to the above equations, the variation in the reliability of the knuckle without detected cracks after service of 400000 km with the service mileage is shown in Figure 12. The service mileage parameters under different reliability levels are listed in Table 7.

It can be concluded from Figure 12 that the RUL of the knuckles that have been in service for 400000 km invisible cracks are detected under different reliability levels is less than the full life of the new knuckles. The RUL prediction model based on the invisible cracks can

reflect the difference in service performance between the old and the new knuckles. In addition, under different reliability levels, the full life of the knuckles that have been in service for 400000 km invisible cracks detected is greater than that of the new knuckles, indicating that the service performance of this knuckle is at the middle and upper level among the new knuckles. It can be seen from Table 7 that when the required reliability is greater than 99.9%, the remaining service mileage of the knuckle is less than 400000 km. It is recommended that a life assessment be carried out based on the crack sizes of the different parts of the steering knuckle detected during maintenance to improved knuckle utilization.

5 Discussions and Verification

Based on the framework proposed in this paper for predicting the RUL of in-service structures with visible and invisible cracks, the RUL of visible cracks at different degrees of reliability and the RUL prediction of the
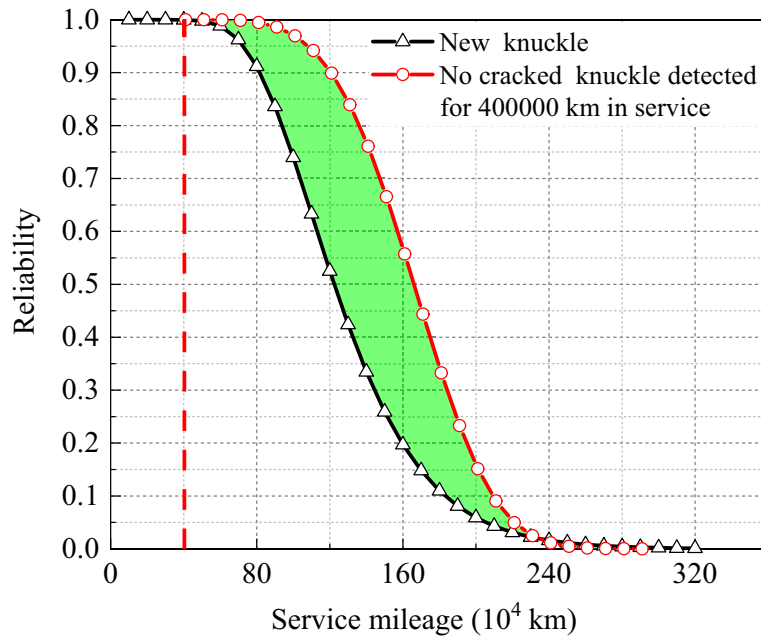

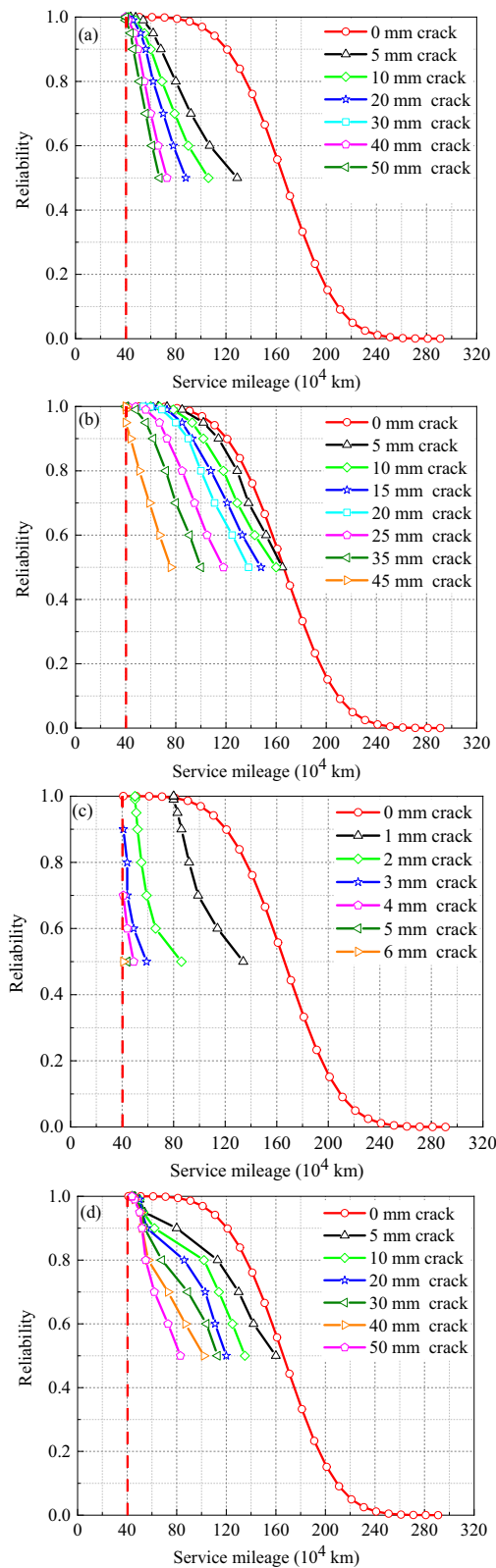**Figure 12** Reliability curve for a knuckle service for 400000 km

Figure 13 Reliability curve for a knuckle in service for 400000 km: (**a**) Mode I (**b**) Mode II (**c**) Mode III (**d**) Mode IV

invisible crack state based on the delay time model is obtained for the knuckle equivalent bench-test fatigue life data in Sections 3 and 4, respectively. Based on the statistical distribution curves of the RUL of visible cracks in Section 3 above, the relationship between the cracks in different regions and the remaining service miles for different failure modes that have been in service for 400000 km can be derived. The RUL for the four methods with varying crack lengths and reliability is calculated based on the cumulative distribution function. The cumulative distribution curves of crack lengths for different life fractions of Figure 9 are taken to obtain the predicted values of RUL for crack sizes with arbitrary reliability and different failure modes.

In Section 4, the reliability RUL prediction curves based on the delay time model are given for the invisible cracked condition of the knuckle. The reliable life of the knuckles that have served 400000 km of invisible cracks is worth the results shown in Figure 12. When high reliability (99.9% or more) is required, the knuckles that have been in service for 400000 km in one section of the repair period are flaw detected. As long as cracks (5 mm) are detected, they cannot meet the service requirements for the next repair cycle. In the case of the four fracture failure modes of the knuckle, Figure 13 compares the crack size states and the reliability RUL curves of the knuckle after 400000 km of service, respectively. The actual service site found that the knuckles in service 400000 km had a crack rate of about 60%~70%, for the remaining 30%~40% of the knuckles did not detect cracks. The RUL of the invisible crack knuckles at 400000 km in service is higher than the knuckle visible cracks, verifying that both methods can guide the life prediction of the actual service structure. Based on the RUL prediction framework proposed in this paper, a life assessment for the knuckle structure in service and utilizing a 400000 km cycle can be carried out. Combined with the crack size found by the actual flaw detection, the RUL prediction curve of visible crack state in different failure areas as shown in Figure 9, is adopted for the knuckle with crack state, and the RUL prediction curve of invisible crack state as shown in Figure 12 is adopted for the knuckle invisible crack state in one cycle of service. Combining the above two states can be selected in Figure 13 under the 99.9% reliability of different crack size curves to realize the dynamic RUL prediction.

6 Conclusions

A hypothetical distributed RUL prediction framework was proposed for visible and invisible cracks in service structures. Considering the structural component of the cast steel knuckles in heavy-duty railway vehicles as the research object, the failure behavior caused by fatigue crack growth is investigated based on the equivalent service load. Crack growth life data under different failure modes of the structure are obtained. The hypothetical distribution framework is employed to predict the statistical evolution characteristics of the crack length and life scores, and the RUL and maintenance suggestions are obtained for different areas, crack sizes, and reliability levels. The main conclusions are as follows:

(1) Based on the crack growth behavior of the knuckle in service, an equivalent service bench test was carried out, and the crack growth life data and distribution rules of the S traction surface and lower traction platform of the knuckle were obtained under different failure modes.

(2) A small amount of nondestructive crack growth life data obtained from equivalent bench tests were synthesized, which considered the overall fitting effect of the data, fatigue failure mechanism and algorithm safety. The cumulative failure probability curves for the crack length and life scores of the knuckle under different modes were obtained. These could be used to evaluate the RUL of a knuckle for a given crack size and reliability.

(3) During the existing state maintenance cycle of the knuckle of 400000 km, once a 5 mm crack is detected, the RUL will not be able to satisfy the next maintenance cycle with 99.9% or more excellent reliability. It is recommended to combine the crack sizes monitored in the operation and maintenance of the actual service knuckle, and realize dynamic RUL prediction by selecting 99.9% reliability curves under different crack sizes according to the RUL prediction methods of visible and invisible cracks.

It should be noted that for the RUL prediction of the crack growth behavior at multiple areas in a complex structure, the crack growth process monitoring data is highly dispersed, and only the typical characteristics of the crack growth failure modes in different regions are considered in this study. Therefore, the current structural condition, mutual influence of multi-site crack growth, and condition process of individual differences should have been considered. The RUL prediction results from the universal application of the equivalent service state. In the future, data-driven algorithms such as neural networks and support vector machines can be used to expand the sample data, build a data-driven condition model based on physical characteristics, and further improve the accuracy of RUL predictions.

Data availability
Data is available according to reasonable request.

Declarations

Competing Interests
The authors declare no competing financial interests.

References
[1] E A Lima, L B Baruffaldi, J L B Manetti, et al. Effect of truck shear pads on the dynamic behavior of heavy haul railway cars. *Vehicle System Dynamics*, 2022, 60(4): 1188-1208.
[2] Q Feng, Z Zhu, Q Tong, et al. Dynamic responses and fatigue assessment of OSD in heavy-haul railway bridges. *Journal of Constructional Steel Research*, 2023, 204: 107873.
[3] C Y Chen, W Li, Y M Liu, et al. Exploration of key traction-running equipment and its problems on heavy-haul trains and research on technology development. *Transportation Safety and Environment*, 2020, 2(3): 161-182.
[4] S Zhao, V Makis, S W Chen, et al. Evaluation of reliability function and mean residual life for degrading systems subject to condition monitoring and random failure. *IEEE Transaction on Reliability*, 2018, 67(1): 13-25.
[5] D I Shishlyannikov, V A Romanov, I E Zvonarev. Determination of the operating time and residual life of self-propelled mine cars of potassium mines on the basis of integrated monitoring data. *Journal of Mining Institute*, 2019, 237: 336-343.
[6] C Wang, T Zhu, B Yang, et al. Remaining useful life prediction framework for crack propagation with a case study of railway heavy duty coupler condition monitoring. *Reliability Engineering & System Safety*, 2023, 230: 108915.
[7] X Ge, L Ling, S Q Chen, et al. Countermeasures for preventing coupler jack-knifing of slave control locomotives in 20,000-tonne heavy-haul trains during cycle braking. *Vehicle System Dynamics*, 2022, 60(9): 3269-3290.
[8] R Serajian, S Mohammadi, A NASR. Influence of train length on in-train longitudinal forces during brake application. *Vehicle System Dynamics*, 2019, 57(2): 192-206.
[9] S P Chunduru, M J Kim, C Mirman. Failure analysis of railroad couplers of AAR type E. *Engineering Failure Analysis*, 2011, 18(1): 374-385.
[10] Z Xu, Q Wu, S Luo, et al. Stabilizing mechanism and running behavior of couplers on heavy haul trains. *Chinese Journal of Mechanical Engineering*, 2014, 27(6): 1211-1218.
[11] C M Sonsino, J Baumgartner, M Breitenberger. Equivalent stress concepts for transforming of variable amplitude into constant amplitude loading

and consequences for design and durability approval. *International Journal of Fatigue*, 2022, 162: 106949.

[12] M Sysyn, U Gerber, F Kluge, et al. Turnout remaining useful life prognosis by means of on-board inertial measurements on operational trains. *International Journal of Rail Transportation*, 2020, 8(4): 347-369.

[13] S C Wu, Z W Xu, Y X Liu, et al. On the residual life assessment of high-speed railway axles due to induction hardening. *International Journal of Rail Transportation*, 2018, 6(4): 218-232.

[14] T Cong, X Liu, S C Wu, et al. Study on damage tolerance and remain fatigue life of shattered rim of railway wheels. *Engineering Failure Analysis*, 2021,123(6): 105322.

[15] K Verbert, B D Schutter, R Babuška. A multiple-model reliability prediction approach for condition-based maintenance. *IEEE Transactions on Reliability*, 2018, 67(3): 1364-1376.

[16] N Zhou, H Wei, H Jiang, et al. Fatigue crack propagation model and life prediction for pantographs on high-speed trains under different service environments. *Engineering Failure Analysis*, 2023, 149: 107065.

[17] M X Yin, T Zhu, J T Xu, et al. Service reliability of a heavy-haul wagon coupler body based on the SMOTE-Bootstrap-Bayes method. *Engineering Failure Analysis*, 2020, 118: 104836.

[18] X Y Ren, S C Wu, H Xing. Fracture mechanics based residual life prediction of railway heavy coupler with measured load spectrum. *International Journal of Fracture*, 2022, 234: 313-327.

[19] Q Feng, F Li, H Li, et al. Hybrid convolution and transformer network for coupler fracture failure pattern segmentation recognition in heavy-haul trains. *Engineering Failure Analysis*, 2023, 145: 107039.

[20] M X Yin, T Zhu, B Yang, et al. Fatigue fracture life of heavy-duty truck coupler based on reliability. *Journal of Mechanical Engineering*, 2021, 57(4): 210-218. (in Chinese)

[21] BS 7910:2019 Guide to methods for assessing the acceptability of flaws in metallic structures, BSI, 2019.

[22] ASME Boiler, Pressure Vessel Committe. ASME boiler and pressure vessel code. Section VIII, Rules for construction of pressure vessels. American Society of Mechanical Engineers, 2015.

[23] J C O Nielsen, T J S Abrahamson, A Ekberg. Probability of instant rail break induced by wheel–rail impact loading using field test data. *International Journal of Rail Transportation*, 2022, 10(1): 1-23.

[24] P Strzelecki. Determination of fatigue life for low probability of failure for different stress levels using 3-parameter Weibull distribution. *International Journal of Fatigue*, 2021, 145: 106080.

[25] M Hassan, F Danish, W B Yousuf, et al. Comparison of different life distribution schemes for prediction of crack propagation in an aircraft wing. *Engineering Failure Analysis*, 2019, 96: 241-254.

[26] F Camci, R B Chinnam. Health-state estimation and prognostics in machining processes. *IEEE Transactions on Automation Science and Engineering*, 2010, 7(3): 581-597.

[27] Y X Zhao, Q Gao, J N Wang. An approach for determining an appropriate assumed distribution of fatigue life under limited data. *Reliability Engineering and System Safety*, 2000, 67(1): 1-7.

[28] J B Ali, B Chebel-Morello, L S Saidi, et al. Accurate bearing remaining useful life prediction based on Weibull distribution and artificial neural network. *Mechanical Systems and Signal Processing*, 2015, 56: 150-172.

[29] B Liu, Y L Teng, Q Huang. A novel imprecise reliability prediction method for incomplete lifetime data based on two-parameter Weibull distribution. *Proceedings of the Institution of Mechanical Engineers*, 2021, 234(1): 208-218.

[30] S Wang, J Gao, C Lin, et al. Condition assessment of high-speed railway track structure based on sparse Bayesian extreme learning machine and Bayesian hypothesis testing. *International Journal of Rail Transportation*, 2023, 11(3): 364-388.

[31] Y Wang, Z X Chen, Y Zhang, et al. Remaining useful life prediction of rolling bearings based on the three-parameter Weibull distribution proportional hazards model. *Insight-Non-Destructive Testing and Condition Monitoring*, 2020, 62(12):710.

[32] Y Zang, S G Wei, B Cai. Hybrid remaining useful life prediction method. A case study on railway D-cables. *Reliability Engineering & System Safety*, 2021, 213: 107746.

[33] Y Fu, X Li, L Huang. Irregular maintenance strategy for offshore wind turbines based on time-delay theory. *Automation of Electric Power Systems*, 2016, 40(15): 133-140.

[34] J J Zhang. Reliability evaluation and opportunistic maintenance policy based on a novel delay time model. *Quality and Reliability Engineering International*, 2018, 35(4): 125-128.

[35] Z Li, F Wang, C Wang. Reliability modeling and evaluation of lifetime delayed degradation process with nondestructive testing. *Reliability Engineering & System Safety*, 2021, 208: 107358.

Chao Wang   born in 1995, is currently a PhD candidate at *State Key Laboratory of Rail Transit Vehicle System, Southwest Jiaotong University, China*. His main research interests include residual life prediction of structures in service.

Tao Zhu   born in 1984, is currently a professor at *State Key Laboratory of Rail Transit Vehicle System, Southwest Jiaotong University, China*. His main research interests include structural design and structural residual life prediction.

Bing Yang   born in 1979, is currently a professor at *State Key Laboratory of Rail Transit Vehicle System, Southwest Jiaotong University, China*. His main research interests include fatigue and fracture.

Shoune Xiao   born in 1964, is currently a professor at *State Key Laboratory of Rail Transit Vehicle System, Southwest Jiaotong University, China*. His main research interests include structural strength and collision dynamics of locomotive and vehicle.

Guangwu Yang   born in 1977, is currently a professor at *State Key Laboratory of Rail Transit Vehicle System, Southwest Jiaotong University, China*. His main research interests include structural design and theory of locomotive and vehicle.